

Article

Highly Efficient and Sustainable ZnO/CuO/g-C₃N₄ Photocatalyst for Wastewater Treatment under Visible Light through Heterojunction Development

Md. Abu Hanif ^{1,*}, Jeasmin Akter ², Young Soon Kim ¹, Hong Gun Kim ^{1,3}, Jae Ryang Hahn ²
and Lee Ku Kwac ^{1,3,*}

¹ Institute of Carbon Technology, Jeonju University, Jeonju 55069, Korea; kyscjb@jj.ac.kr (Y.S.K.); hkim@jj.ac.kr (H.G.K.)

² Department of Chemistry, Research Institute of Physics and Chemistry, Jeonbuk National University, Jeonju 54896, Korea; tina44445@gmail.com (J.A.); jrhanh@jbnu.ac.kr (J.R.H.)

³ Graduate School of Carbon Convergence Engineering, Jeonju University, Jeonju 55069, Korea

* Correspondence: hanif4572@gmail.com (M.A.H.); kwac29@jj.ac.kr (L.K.K.);
Tel.: +82-63-220-3157 (M.A.H.); +82-63-220-3063 (L.K.K.)

Abstract: Dye-containing pollutants are currently a threat to the environment, and it is highly challenging to eliminate these dyes photocatalytically under visible light. Herein, we designed and prepared a ZnO/CuO/g-C₃N₄ (ZCG) heterostructure nanocomposite by a co-crystallization procedure and applied it to eliminate pollutants from wastewater via a photocatalytic scheme. The structural and morphological features of the composite confirmed the formation of a ZCG nanocomposite. The photocatalytic capability of the ZCG photocatalyst was investigated via the decomposition of methylene blue dye. The outstanding activity level of 97.46% was reached within 50 min. In addition, the proficiency of the ZCG composite was 753%, 392%, 156%, and 130% higher than photolysis, g-C₃N₄, CuO, and ZnO, respectively. Furthermore, the photodeterioration activity on Congo red was also evaluated and found to be excellent. The enhanced catalytic achievement is attributed to the construction of heterojunctions among the constituent compounds. These properties boost the charge transfer and decrease the recombination rate. Moreover, the reusability of the ZCG product was explored and a negligible photoactivity decline was detected after six successful runs. The outcomes suggest the as-prepared nanocomposite can be applied to remove pollutants, which opens a new door to practical implementation.

Keywords: ZnO/CuO/g-C₃N₄; co-crystallization; heterojunction; photocatalytic degradation; organic pollutant



Citation: Hanif, M.A.; Akter, J.; Kim, Y.S.; Kim, H.G.; Hahn, J.R.; Kwac, L.K. Highly Efficient and Sustainable ZnO/CuO/g-C₃N₄ Photocatalyst for Wastewater Treatment under Visible Light through Heterojunction Development. *Catalysts* **2022**, *12*, 151. <https://doi.org/10.3390/catal12020151>

Academic Editors: Florica Papa, Anca Vasile and Gianina Dobrescu

Received: 29 December 2021

Accepted: 21 January 2022

Published: 25 January 2022

Publisher's Note: MDPI stays neutral with regard to jurisdictional claims in published maps and institutional affiliations.



Copyright: © 2022 by the authors. Licensee MDPI, Basel, Switzerland. This article is an open access article distributed under the terms and conditions of the Creative Commons Attribution (CC BY) license (<https://creativecommons.org/licenses/by/4.0/>).

1. Introduction

In recent years, environmental pollution has become a severe problem for human health and aquatic life due to industrialization and the use of a massive amount of chemicals. The pollutants that arise from industries, including food coloring, dyeing, printing, and textiles, which contain various types of untreated dyes, are released directly into water bodies. Among several dyes used, methylene blue (MB) is a cationic dye, and it is applied on a vast scale as a colorant material in industries. People who come into contact with MB face acute illness, especially abdominal pain, nausea, headache, corneal injury, dizziness, and anemia, as well as it being detrimental for aquatic and other organisms [1]. In addition, Congo red (CR) is also a noxious anionic azo dye. CR is widely used in textile industries, as a pH indicator, and in the diagnosis of amyloidosis and benzidine metabolization, etc. This toxic dye is responsible for dangerous diseases such as gastrointestinal and eye disorders and skin irritations, and causes allergic and respiratory problems [2]. Hence, it is necessary to eliminate the harmful dyes from wastewater before mixing them into the

aquatic environment. However, the decolorization technique is very challenging due to the complex structure of the dyes. This is why numerous research teams are trying to find a sustainable method to resolve this serious issue. The traditional approaches, including adsorption, sand filtration, coagulation/flocculation, precipitation, biodegradation, etc., are familiar methods used to eradicate the contaminants from wastewater [3,4]. Nevertheless, the sustainability of most of these conventional methods is in doubt because they require a huge amount of catalyst. Additionally, such procedures may generate huge amounts of secondary pollutants or convey one form to another form. Conversely, advanced oxidation processes such as ozonation, photocatalysis, Fenton oxidation might be the next generation step for wastewater treatment systems. In particular, the photocatalytic method is an appropriate process in respect of sustainability. Moreover, it is more appropriate than others due to its better performance, lack of secondary pollutant formation, low cost, easy operation, and eco-friendliness. The harmful pollutants are converted into various non-toxic products such as carbon dioxide and water with the assistance of reactive oxygen species in the photocatalysis system [1]. However, selection of a suitable photocatalyst is a vital concern for enhancing deterioration proficiency.

Currently, semiconductor-based photocatalysts have been explored extensively in various fields using methods such as water splitting, supercapacitors, removal of pollutants from wastewater by photocatalysis, H₂ production, CO₂ reduction, and so on. The increasing attention being paid to the use of semiconductor materials is due to their electronic structure. Among the widely used semiconductor photocatalysts, ZnO and CuO are most significantly applied due to being low cost and non-toxic, with notable thermal and electrical conductivity and outstanding photocatalytic efficiency. Nonetheless, these two materials, when used alone, have some inconvenient limitations in visible light photocatalytic applications. In general, the photodecomposition proficiency of ZnO and CuO alone is minimal due to insufficient visible light harvesting and the high recombination rate of photoinduced electron-hole (e^- - h^+) pairs, low surface area, and low electron charge separation [5–8]. In contrast, ZnO and CuO enhance their catalytic activity by working as a supporting material through heterojunction construction [7,9]. These heterojunctions and hierarchical nanostructures diminish the recombination rate and enhance the photocatalytic activity of the composite materials compared with pure oxides [10–13]. Although the ZnO/CuO composite showed greater photodegradation proficiency than the separated ZnO or CuO compounds, we found that the catalytic activity of ZnO/CuO material did not gain a satisfactory level for practical implementation via visible light irradiation [9,14–16]. Therefore, the ZnO/CuO composite needs to be further coupled with an electrically conducting material to increase its photodegradation ability under visible light irradiation. Thus, it remains a challenge to discover the appropriate photocatalytic compound which will improve the VL photocatalytic activity.

Based on the above hypothesis, graphitic carbon nitride (g-C₃N₄) might be a suitable compound for coupling with the ZnO/CuO composite because of its low cost and large-scale manufacturing, unique electronic and optical properties, good chemical and thermal stability, facile preparation, and non-toxicity [17,18]. In addition, the photocatalytic activity of g-C₃N₄-related composites has been extensively studied [19–23]. However, the photocatalytic efficiency towards pollutant degradation of pristine g-C₃N₄ is low due to its quick e^- - h^+ pair recombination ability [18,24]. Therefore, to counteract this drawback, various methods have been applied in attempts to increase the visible light photocatalysis, particularly coupling with other semiconductors or metals, non-metal doping, control of morphology, etc.

In this work, we focused on the preparation of a ZnO/CuO/g-C₃N₄ (ZCG) nanocomposite through an efficient co-crystallization method and executed the photocatalytic process for the treatment of dye-containing wastewater followed by visible light irradiation. Our synthesis process may open a new way to prepare other g-C₃N₄-based semiconductor composites in the near future. The physicochemical properties of the as-synthesized ZCG nanocomposite were systematically investigated by using various spectroscopic and

microscopic techniques. The ZCG nanocomposite showed excellent photocatalytic MB deterioration activity compared with g-C₃N₄, ZnO, CuO, and with photolysis under visible light illumination. Additionally, the photocatalytic ability of the ZCG heterostructure for the photodegradation of CR dye was also evaluated and showed remarkable efficiency. The enhanced activity that was achieved may be due to the heterojunction construction among g-C₃N₄, ZnO, and CuO compounds, which suppressed the recombination rate of the photoinduced $e^- - h^+$ pairs and enhanced the flow of e^- transfer. In addition, in order to understand the recyclability and stability of the as-synthesized ZCG composite, we explored the recycling ability up to six times along with XRD and FTIR analysis before and after photodegradation. There were no significant changes in photocatalytic activity and structural properties during recycling, which strongly implies the possibility for the practical implementation of our work. The probable photocatalytic degradation mechanism was also discussed.

2. Results and Discussion

2.1. Structural Characterization

The crystal structure of the as-prepared g-C₃N₄, CuO-NPs, ZnO-NPs, and ZCG composite was inspected by X-ray diffraction (XRD) and is presented in Figure 1. The XRD pattern of the g-C₃N₄ confirms two peaks (Figure 1a): one is at 12.77° corresponding to the (100) plane of the inter-planar stacking of a tri-s-triazine unit and the other one is at 27.74° and belongs to the (002) plane due to the interplanar stacking of the conjugated aromatic system (JCPDS 87-1526). The diffraction peaks of CuO-NPs are positioned at 32.43°, 35.46°, 38.63°, 48.68°, 53.36°, 58.28°, 61.45°, 66.14°, and 67.96° (Figure 1b) and correspond to the crystal planes (110), ($\bar{1}11$), (111), ($\bar{2}02$), (020), (202), ($\bar{1}13$), ($\bar{3}11$), and (113), respectively, with monoclinic morphology (JCPDS 96-901-5569). The ZnO-NPs diffraction peaks were detected at 31.51°, 34.18°, 35.96°, 47.34°, 56.39°, 62.66°, 66.22°, 67.81°, and 67.81° for the (100), (002), (101), (102), (110), (113), (200), (112), and (201) facets, respectively (Figure 1c). All of the diffraction peaks of the ZnO-NPs were matched with the ZnO hexagonal wurtzite structure (JCPDS 36-1451). All the characteristic diffraction peaks of g-C₃N₄, CuO-NPs, and ZnO-NPs appeared in the ZCG nanocomposite, confirming its successful formation (Figure 1d). No additional peaks were found in the composite, indicating the as-prepared ZCG nanocomposite is highly pure.

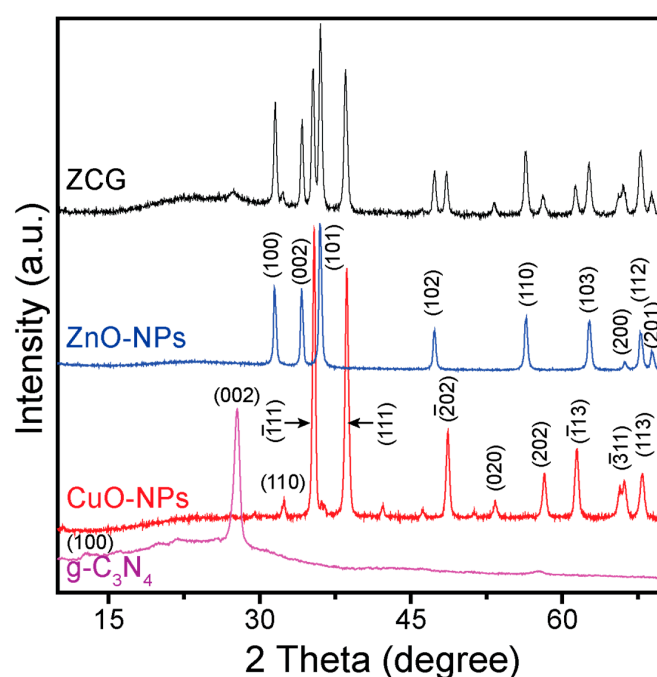


Figure 1. XRD spectra of the (a) g-C₃N₄, (b) CuO-NPs, (c) ZnO-NPs, and (d) ZCG nanocomposite.

The crystallite size (D) of the CuO-NPs, ZnO-NPs, and ZCG nanocomposite was calculated applying Scherrer's formula ($D = \frac{k\lambda}{\beta \cos \theta}$, where k denotes non-dimensional shape factor (0.94), β is the full width at half maximum, λ is the X-ray wavelength, and θ is the Bragg angle). In this case, all the above-mentioned planes were used to calculate the average D of the materials. The average D values of the CuO-NPs, ZnO-NPs, and ZCG nanocomposite were 22.46, 21.26, and 20.37 nm, respectively. Further, the D values of the CuO-NPs, ZnO-NPs, and ZCG nanocomposite were verified by using the modified Scherrer equation and the corresponding curves are shown in Figure S1. The calculated D values of the CuO-NPs, ZnO-NPs, and ZCG nanocomposite were 27.01, 26.45, and 25.32 nm, respectively (described in Supplementary File in detail). There is little difference in the results and the order of crystallite size (CuO-NPs > ZnO-NPs > ZCG) is the same.

The binding energy, valence state, and purity of the ZCG nanocomposite were analyzed by X-ray photoelectron spectroscopy (XPS) and are shown in Figure 2. Figure 2a indicates the survey spectrum of the composite and affirms the presence of Zn, Cu, O, N, and C elements in the composite. The high-resolution Zn 2p plot was observed at binding energies of 1021.37 and 1044.37 nm for Zn-2p_{3/2} and Zn-2p_{1/2} chemical environments, respectively (Figure 2b). These results imply the existence of a Zn²⁺ oxidation state in the ZCG nanocomposite. In addition, the difference between the mentioned peaks is 23.0 eV, confirming the oxidation state of the Zn in the composite is +2 [25]. Figure 2c displays the XPS features of the Cu 2p. The peaks at 952.64 and 932.68 eV were allotted for Cu-2p_{1/2} and Cu-2p_{3/2} of CuO. In addition, the satellite peaks were found to be 940.63, 943.32, and 961.71 eV, confirming the presence of a partially filled d orbital ($3d^9$) of Cu²⁺ in the nanocomposite [1]. The two deconvoluted peaks of O 1s were positioned at 529.31, and 530.79 eV, respectively (Figure 2d). These characteristic peaks are observed due to the lattice oxygen (O²⁻) and adsorbed molecular oxygen on the surface of the ZCG composite [26,27]. The core-level spectra of N 1s are shown in Figure 2e. The three deconvoluted bands at binding energies of 400.75, 399.70, and 398.31 eV correspond to the amino functions (C–N–H), tertiary nitrogen N–(C)₃, and sp^2 -bonded triazine rings (C–N=C), respectively [28,29]. The deconvoluted high-resolution XPS spectrum of C-1s (Figure 2f) was exhibited at 284.39, 285.46, and 287.86 eV. The peak at 287.86 eV is attributed to sp^2 -coordinated carbon-containing aromatic rings (N–C=N) [30]. The peak located at 285.46 eV is due to C–O species on the surface of g-C₃N₄ [28,31]. The peak centered at a binding energy of 284.6 eV is ascribed to sp^2 -hybridized C–C bonds. Therefore, XPS investigation suggested that the ZCG nanocomposite was composed of g-C₃N₄, ZnO, and CuO, and confirmed their successful combination in the composite.

The nature of the chemical bonding and functional groups of g-C₃N₄, ZnO-NPs, CuO-NPs, and the ZCG nanocomposite were studied through Fourier transform infrared spectroscopy (FTIR) and are demonstrated in Figure 3. Figure 3a shows the characteristic peaks of g-C₃N₄. The peak that appears at 805 cm⁻¹ is due to the breathing mode of the s -triazine ring [28]. A series of bands at approximately 1218, 1315, 1411, and 1551 cm⁻¹ are related to the stretching vibrations of aromatic C–N heterocycles, and the peak at 2118 cm⁻¹ is observed for an asymmetric stretching mode of cyano groups (C≡N) [32]. The absorption band around 449 cm⁻¹ corresponds to the Zn–O stretching vibration (Figure 3b). The peak centered between 400 and 555 cm⁻¹ is attributed to the ZnO hexagonal structure [25]. Figure 3c represents the FTIR curve of CuO-NPs and the most significant peaks are found at 585 and 531 cm⁻¹, corresponding to the stretching vibrational mode of Cu–O bonds associated with the plane ($\bar{1}01$), and (101), respectively [33]. In addition, the wide band between 3000–3500 cm⁻¹ is ascribed for all the compounds as a result of the stretching mode of O–H from the atmosphere. All the demonstrative bands are evident in the spectrum of the ZCG composite (Figure 3d), further confirming the coexistence of ZnO, CuO, and g-C₃N₄.

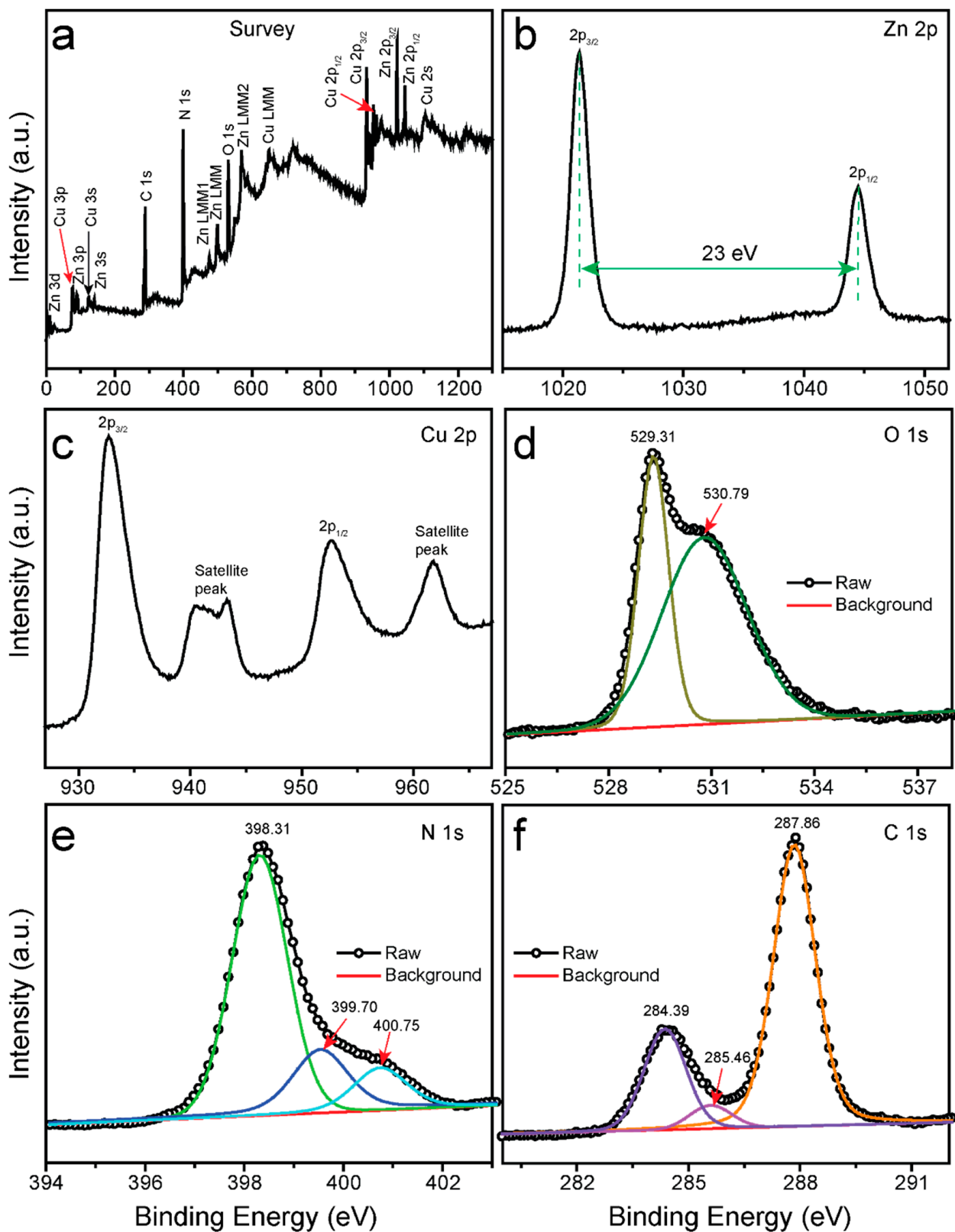


Figure 2. XPS spectra of ZCG nanocomposite. (a) Survey; (b–f) High-resolution spectra of Zn 2p, Cu 2p, O 1s, N 1s, and C 1s, respectively.

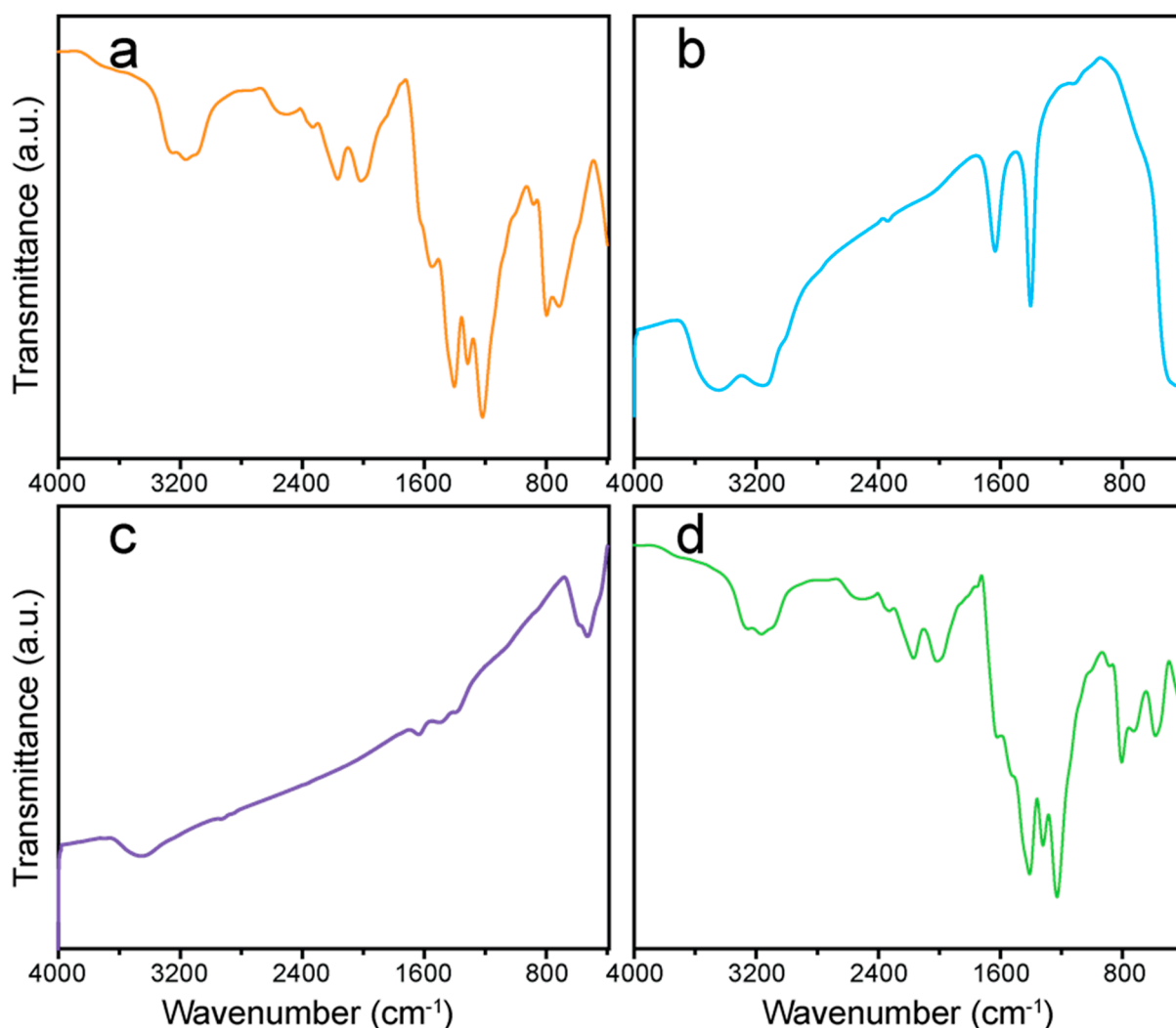


Figure 3. FTIR spectra of the (a) $g\text{-C}_3\text{N}_4$, (b) ZnO-NPs, (c) CuO-NPs, and (d) ZCG nanocomposite.

2.2. Optical Characterization

The optical characteristics of the material are a crucial parameter in the application as a photocatalyst. UV-vis spectroscopy was applied to determine the optical features of the $g\text{-C}_3\text{N}_4$, ZnO-NPs, CuO-NPs, and ZCG nanocomposite. The absorption edge of the $g\text{-C}_3\text{N}_4$, ZnO-NPs, CuO-NPs, and ZCG nanocomposite indicates that all the samples can be used in the visible region of light. In addition, their corresponding bandgap energy (E_g) was calculated by using Tauc plots (Figure 4). The E_g of the materials was measured via extrapolation of the $(\alpha h\nu)^2$ vs. E , where $h\nu$ refers to photon energy ($1239/\lambda$, in eV) and α represents the absorption coefficient. The intercept of the E axis where $(\alpha h\nu)^2 = 0$ gives the E_g value. The calculated E_g values of the $g\text{-C}_3\text{N}_4$, ZnO-NPs, CuO-NPs, and ZCG nanocomposite were 2.33, 2.25, 1.46, and 1.69 eV, respectively. Interestingly, after the construction of the nanocomposite, the E_g value was noticeably lower than that of the individual compounds except CuO-NPs. The reduced E_g of the composite facilitates the $e^- - h^+$ pair generation and minimizes their recombination rate. In general, the lower the E_g value, the higher the photocatalytic activity of the material. Although the bandgap of the pure CuO is smaller than those of the nanocomposites, the pure CuO showed low photocatalytic efficiency. This is due to the photocatalytic efficiency also being sensitive to several factors, such as crystalline size, heterojunction formation, and charge recombination effect. The ZCG composite showing higher photocatalytic activity than the single CuO could be due to the modification of surface morphology such as heterojunction development, and the small crystallite size of the nanocomposite.

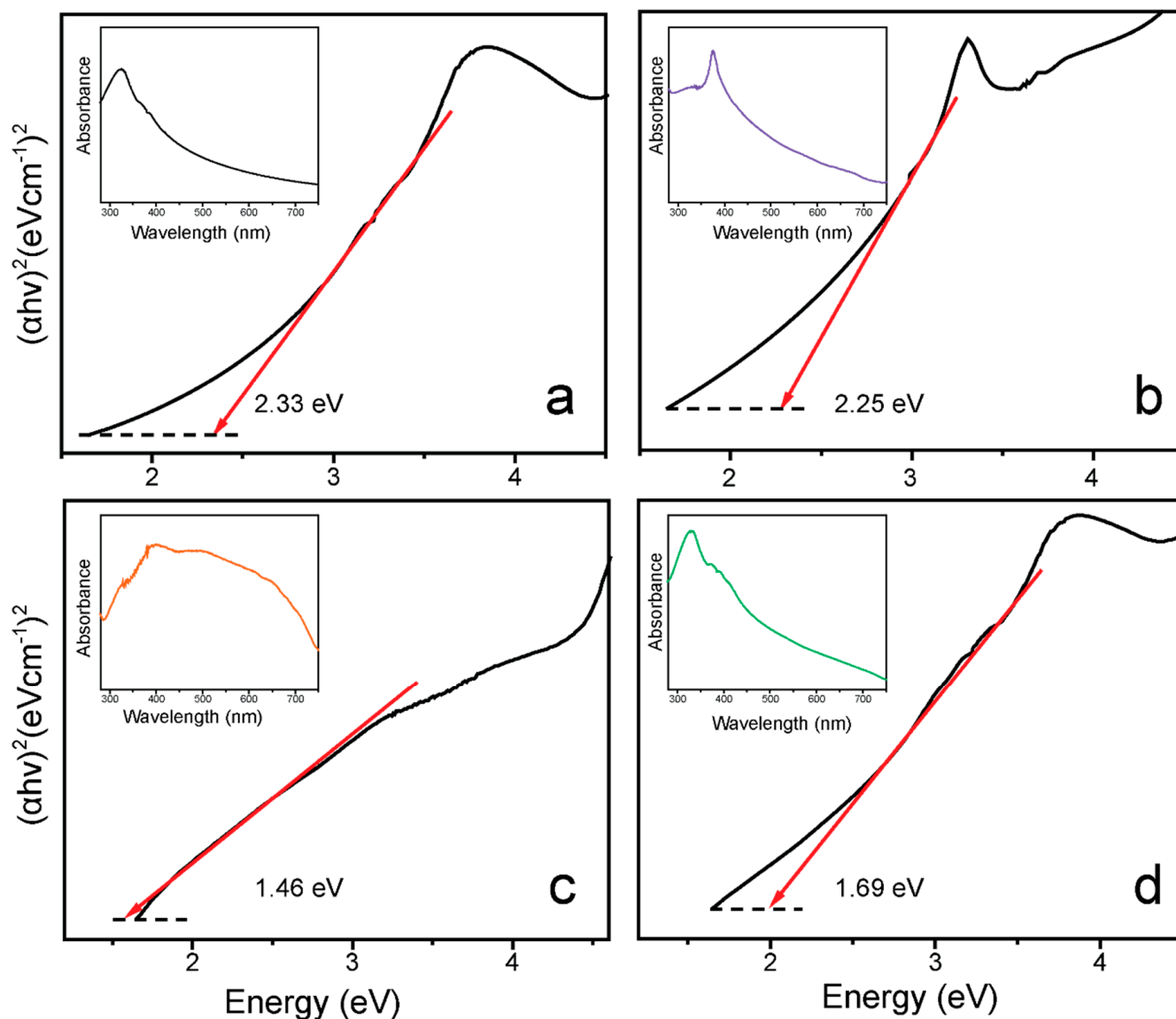


Figure 4. Tauc plots of the (a) $g\text{-C}_3\text{N}_4$, (b) ZnO-NPs, (c) CuO-NPs, and (d) ZCG nanocomposite. Each inset displays the representative UV-vis absorption data of the compound.

2.3. Morphological Investigation

The morphological features of the as-prepared $g\text{-C}_3\text{N}_4$, CuO-NPs, ZnO-NPs, and ZCG nanocomposite were analyzed by field-emission scanning electron microscopy (FE-SEM) and are depicted in Figure 5. Figure 5a shows the structure of as-synthesized $g\text{-C}_3\text{N}_4$ is aggregated, thin, and a flat sheet. The as-constructed ZnO-NPs are nanorod-shaped structures and the size and shape of the nanorods are almost uniform throughout the compounds (Figure 5b). Figure 5c displays the spherical-shaped CuO-NPs. The size of the CuO-NPs lies between 64 and 180 nm and the average size is approximately 98 nm (forty-five particles are counted). The ZCG nanocomposite is composed of three types of morphology: sheet-like $g\text{-C}_3\text{N}_4$, nanorod-like ZnO, and sphere-like CuO (Figure 5d). These results indicate the successful formation of a ZCG heterostructure nanocomposite with a C_3N_4 , ZnO, and CuO chemical environment. Such types of heterostructure enhance the electron flow and reduce the recombination rate and, therefore, improve the photocatalytic efficiency of the product [34].

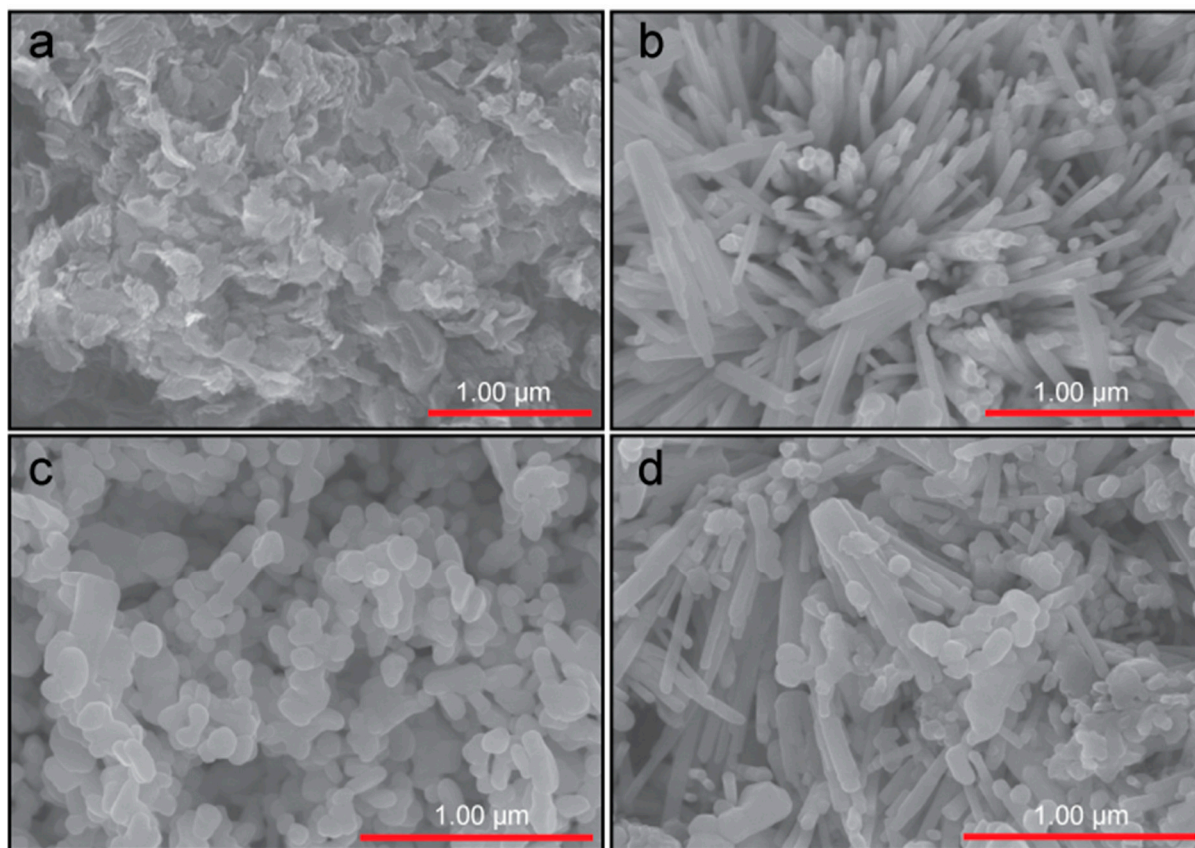


Figure 5. FE-SEM images of the as-synthesized (a) $g\text{-C}_3\text{N}_4$, (b) ZnO-NPs, (c) CuO-NPs, and (d) ZCG nanocomposite.

For a better understanding of the heterostructure, we further used high-resolution transmission electron microscopy (HR-TEM) to explain the presence of $g\text{-C}_3\text{N}_4$, ZnO, and CuO nanoparticles in the ZCG composite. Figure 6a,b show the low and high magnification micrographs of the compound. As can be clearly seen from both the figures, the ZCG nanocomposite is constructed by $g\text{-C}_3\text{N}_4$, ZnO, and CuO compounds and their individual morphology is intact after forming the composite. The outcomes are also balanced with the findings of FE-SEM.

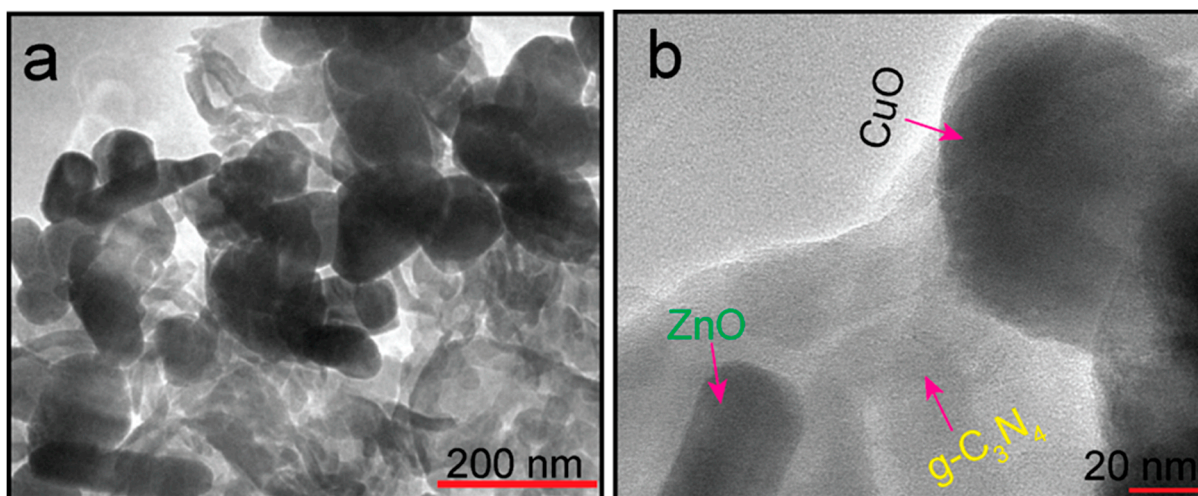


Figure 6. (a) Low and (b) high resolution micrographs of the ZCG nanocomposite.

The chemical confirmation and purity of the as-prepared ZCG nanocomposite were analyzed through energy-dispersive X-ray spectroscopy (EDS) and are shown in Figure 7a,b. Figure 7a from the FE-SEM image was used to determine the EDS analysis. The result shows that the five constituent elements Zn, Cu, O, C, and N exist in the composite and their atomic and weight percentages (inset) are indicated in Figure 7b. The prepared nanocomposite is free from impurities due to the absence of additional peaks. These findings are in line with the XRD outcomes. The distribution of the elements in the composite was further inspected using elemental mapping images of the ZCG composite (Figure 7c,d). The outcomes confirm that the Zn, Cu, O, N, and C elements were homogeneously distributed in the nanocomposite.

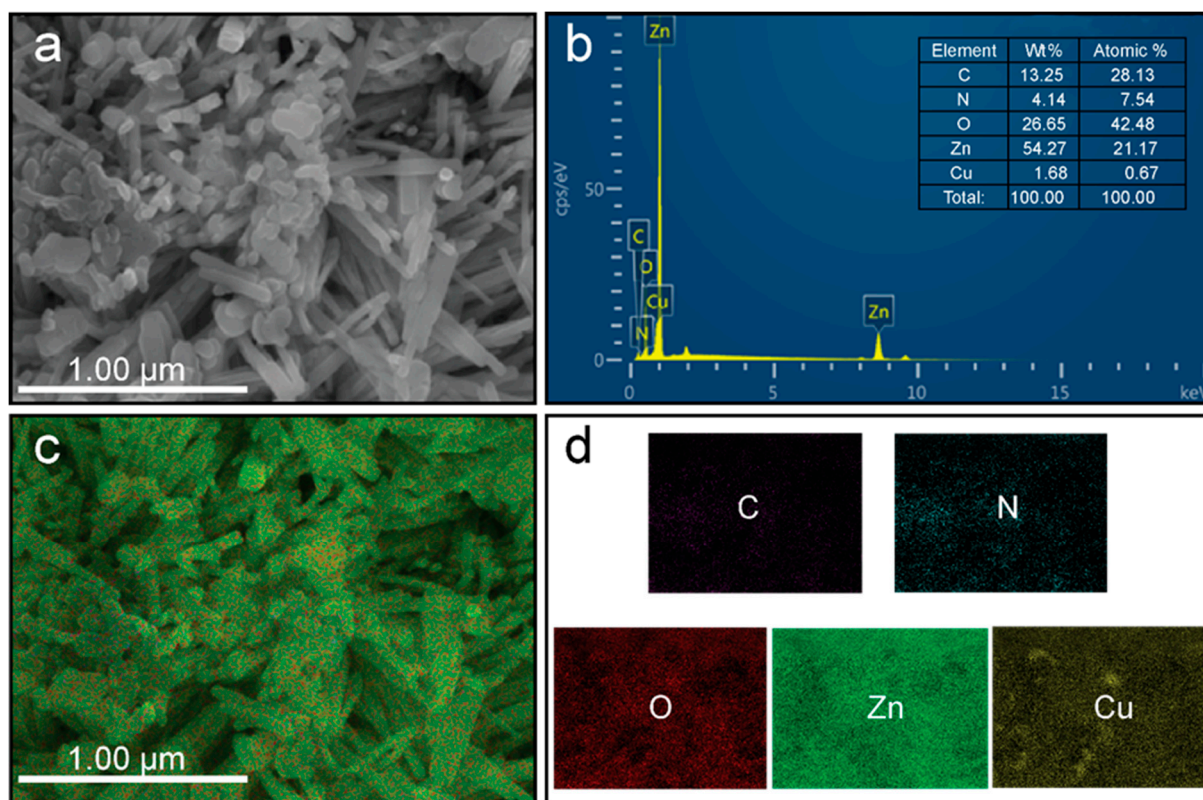


Figure 7. (a,b) EDS and (c,d) elemental mapping analysis of the ZCG nanocomposite.

2.4. Photocatalytic Assessment of the Compounds

The photodegradation activity of $g\text{-C}_3\text{N}_4$, ZnO-NPs, CuO-NPs, ZCG, and photolysis (PL) was evaluated for the deterioration of MB as a representative organic pollutant under visible light illumination for 50 min. The adsorption ability was also inspected under dark conditions and is displayed in Figure 8a. The results show the adsorption proficiency of the compounds is negligible compared with photodegradation and increase in sequence $\text{PL} < g\text{-C}_3\text{N}_4 < \text{CuO-NPs} < \text{ZnO-NPs} < \text{ZCG}$. The photocatalytic activity of the aforementioned materials was calculated through the following Equation (1) [35]:

$$\eta(\%) = \left(\frac{C_0 - C_t}{C_0} \right) \times 100 \quad (1)$$

where η refers to the degradation ability, and C_t and C_0 express the absorbance at t and 0 min, respectively. Figure 8a shows the photodegradation efficiency of all the investigated samples along with PL. The as-constructed ZCG composite shows the highest efficiency (97.46%) within 50 min of visible light stimulation. The catalytic activity was enhanced in the order $\text{PL} (12.95\%) < g\text{-C}_3\text{N}_4 (24.88\%) < \text{CuO-NPs} (62.09\%) < \text{ZnO-NPs} (75.37\%) <$

ZCG (97.46%). The photocatalytic activity of the ZCG nanocomposite was 753%, 392%, 156%, 130% higher than that of PL, g-C₃N₄, CuO-NPs, and ZnO-NPs, respectively. In addition, as can be realized from Figure 8a, the activity of the ZCG composite gradually increased after the introduction of g-C₃N₄, CuO-NPs, and ZnO-NPs materials. Further, the reduced catalytic ability of g-C₃N₄, CuO-NPs, and ZnO-NPs is observed because of the quick recombining impact of photoinduced e^-h^+ pairs in these substances. Conversely, the enhanced efficiency of the ZCG composite followed due to the heterostructure development in the composite which suppressed the recombination effect.

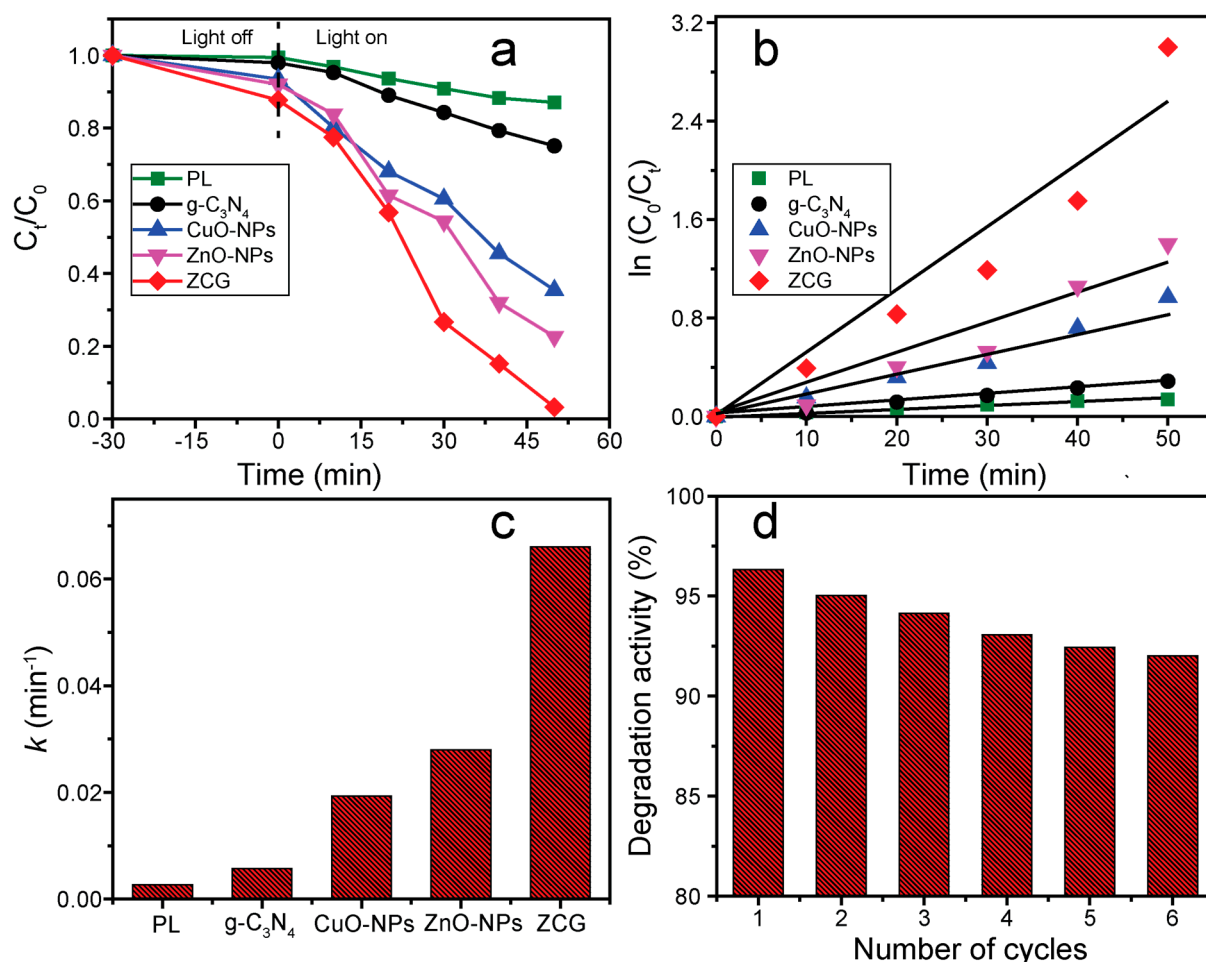


Figure 8. (a) Degradation proficiency as a function of time, (b) Corresponding kinetics curves, (c) Estimated rate constant, (d) Recyclability of the ZCG nanocomposite.

Further, a kinetics study was undertaken to better understand the product's catalytic activity, as shown in Figure 8b. The linear plots of $\ln(C_0/C_t)$ vs. illumination time for MB photodegradation show pseudo-first-order reaction kinetics. The deterioration rate constant (k) was calculated employing Equation (2) [35]:

$$\ln\left(\frac{C_0}{C_t}\right) = kt \quad (2)$$

where t represents the irradiation time of the reaction. Figure 8c shows the k values for PL, g-C₃N₄, CuO-NPs, ZnO-NPs, and ZCG were 0.0028, 0.0057, 0.0193, 0.0280, and 0.0660 min^{-1} , respectively. The ZCG composite demonstrated the highest k value compared to other inspected materials. This value is 23.6 times greater than without the catalyst (PL). Even the k value of the ZCG nanocomposite is 11.6, 3.4, and 2.4 times larger than the g-C₃N₄, CuO-NPs, and ZnO-NPs compounds, respectively. The k value of the as-prepared

ZCG nanocomposite is enhanced compared with those of the single materials $g\text{-C}_3\text{N}_4$, CuO-NPs, and ZnO-NPs used for MB photodegradation via visible light irradiation. Hence, the composite materials display a vital property for boosting the photocatalytic activity and rate constant compared with single materials applied in the reaction.

To reduce wastewater treatment costs and prevent the generation of secondary pollutants, photocatalysts with excellent reusability and high stability are highly recommended for research. The recyclability and constancy of the ZCG catalyst were investigated in as many as six successive runs of MB photodegradation upon 50 min visible light irradiation. As can be observed from Figure 8d, the photocatalytic ability of the ZCG nanocomposite exhibited a negligible decreasing efficiency after six cycles, which might be due to the damage caused by the catalyst throughout the recycling procedure. In addition, the structural changes of the ZCG composite were evaluated by XRD and FTIR instruments before and after (six cycles) catalytic reaction (Figure 9). The outcomes confirm that there are no substantial structural changes on the nanocomposite after the reaction. Therefore, our as-synthesized ZCG composite revealed remarkable reusability and stability which can be applied to the decomposition of organic pollutants under visible light.

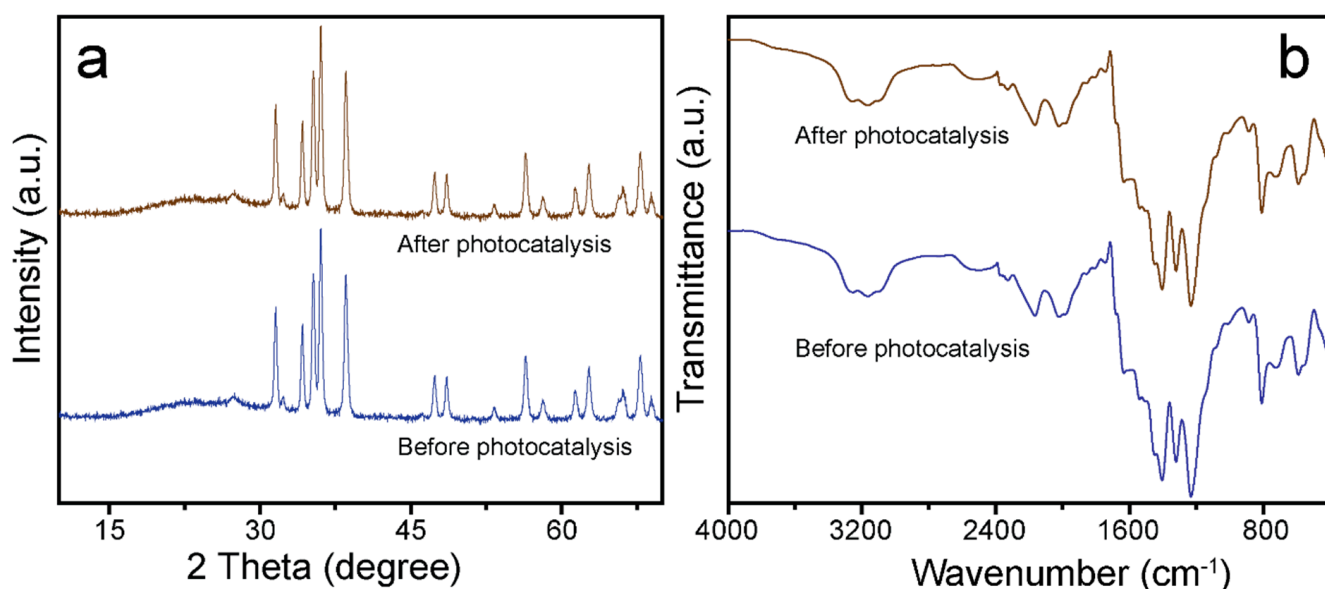


Figure 9. (a) XRD, and (b) FTIR patterns of the ZCG nanocomposite (before, and after photocatalytic analysis).

The photocatalytic efficiency of the as-synthesized ZCG nanocomposite was also studied to evaluate the degradation capability of other organic pollutants. Herein, CR was used to analyze its photodeterioration ability under identical experimental conditions. The catalytic potency of the ZCG composite was found to be 91.73% for the degradation of CR dye within 50 min (Figure 10a). Further, the kinetics analysis was evaluated and is shown in Figure 10b. The result indicates that pseudo-first-order kinetics was followed for the deterioration of CR. The estimated k value of the composite was 0.0371 min^{-1} . Therefore, the photodegradation efficiency of the as-prepared ZCG composite is noticeably higher compared with the previously described composite.

Table 1 displays the photocatalytic activity of the previously reported compounds and as-synthesized ZCG nanocomposite. The assessment indicates that our as-prepared ZCG composite is highly suitable for application in wastewater treatment compared with the other materials.

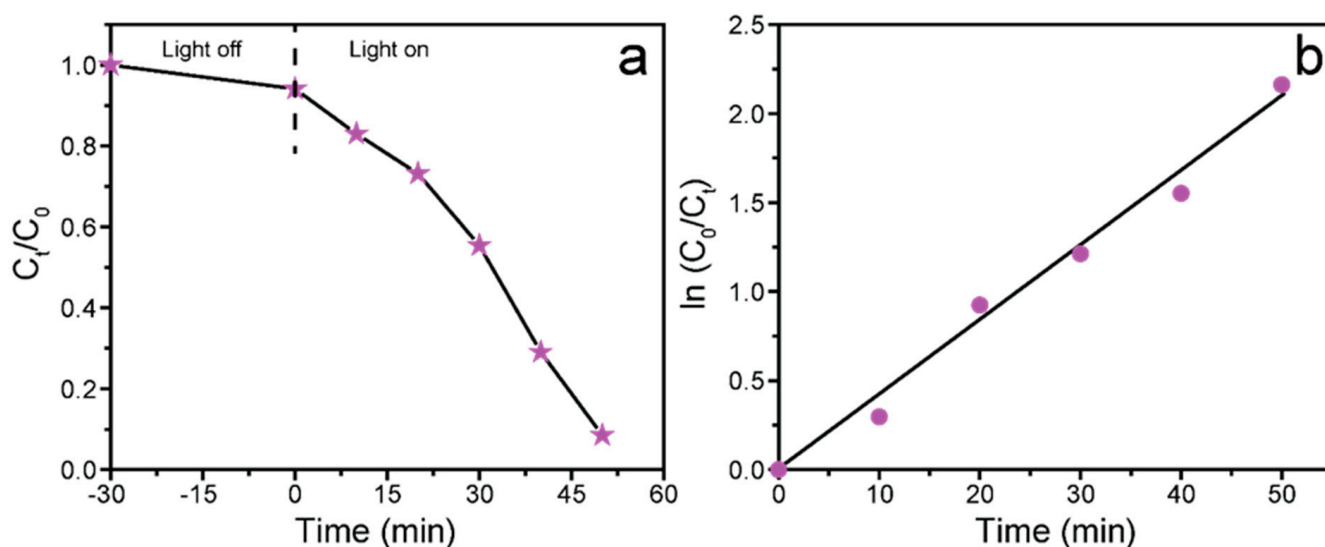


Figure 10. (a) Photocatalytic proficiency of the ZCG nanocomposite for the deterioration of Congo red, and (b) corresponding kinetics plot.

Table 1. Comparison of the photocatalytic decomposition of as-synthesized ZCG composite and ZnO/CuO or g-C₃N₄-based composite.

Catalyst	Pollutant (Dye)	Dye Dose	Catalyst Dose (g)	Degradation (%)	Time (min)	Ref.
ZnO/CuO	MB	10 ppm	0.01	73	120	[9]
ZnO/CuO	MB	3×10^{-5} ML ⁻¹	0.5	97.2	120	[14]
ZnO/CuO	MB	6 mg L ⁻¹	0.4 g L ⁻¹	82	120	[15]
ZnO/CuO	MB	20 mg L ⁻¹	0.5 g L ⁻¹	93	120	[16]
ZnO/ZnS/g-C ₃ N ₄	MB	100 mL, 10 mg L ⁻¹	0.05	75	60	[36]
Fe ₂ O ₃ -xS _x /S-doped g-C ₃ N ₄	MB	100 mL, 8 mg L ⁻¹	0.07	82	150	[37]
Ba/Alg ¹ /CMC ² /TiO ₂	CR	4.3×10^{-5} M	1.2 L ⁻¹	91.5	240	[38]
ZnO/CuO/g-C ₃ N ₄ (ZCG)	MB	100 mL, 20 mg L ⁻¹	0.02	97.46	50	Our work
	CR	100 mL, 20 mg L ⁻¹	0.02	91.73		

¹ Alg = alginate, ² CMC = carboxymethyl.

2.5. Determination of the Point of Zero Charge (pH_{pzc}) and pH Effect

The electrical charge and pH of the catalyst and organic pollutants are vital parameters for understanding photocatalytic efficiency. The pH_{pzc} signifies the charge of the catalyst surface. The pH drift technique was applied to estimate the pH_{pzc} of the as-prepared ZCG composite. The initial pH (pH_i) of the solution was adjusted by adding either HCl or NaOH. The final pH (pH_f) was then measured. The pH_{pzc} was determined by plotting pH_i vs ΔpH ($pH_f - pH_i$) and pH_{pzc} refers to the point at which the total numbers of positive and negative charges are identical. The pH_{pzc} of the ZCG nanocomposite was 7.36 (Figure 11a). These outcomes indicate that the ZCG catalyst's surface is negative at pH values higher than pH_{pzc} and positive at pH values lower than pH_{pzc} . The pH effect of the ZCG composite for the MB deterioration was investigated at different pH values (pH 3, 6, 9, and 12). In addition, the catalyst dose and concentration of the solution in each experiment were identical. The photocatalytic proficiency of the composite was dramatically improved with the increase in the solution's pH (Figure 11b). The highest activity was achieved at a high pH (12, basic medium) within 30 min due to the strong interaction between the

cationic MB dye and the anionic (negatively charged) surface of the catalyst. By contrast, the lowest efficiency was observed at pH 3 because at low pH (acidic medium), the catalyst surface behaves with a cationic nature and therefore repulsion takes place between MB and the catalyst surface.

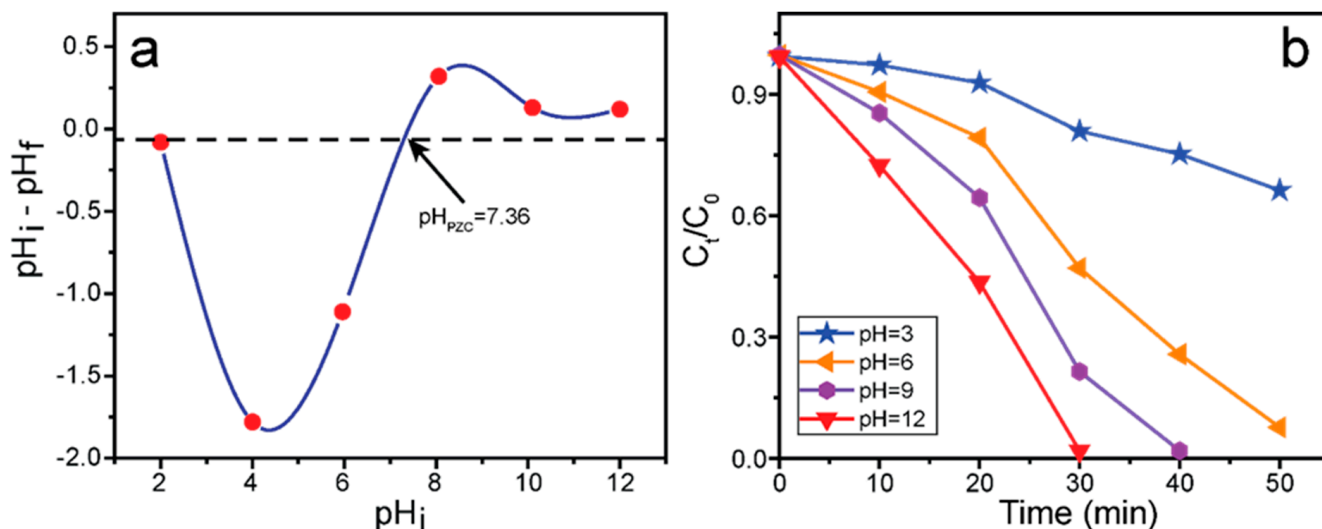
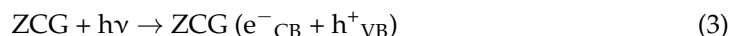


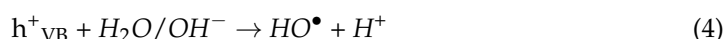
Figure 11. (a) Point of zero charge, and (b) pH effect on the deterioration of MB under VL using ZCG nanocomposite.

2.6. Proposed Photocatalytic Degradation Mechanism

When the ZCG nanocomposite is exposed to VL irradiation, photoinduced holes (h^+) and electrons (e^-) are produced on its surface by absorption of photons (Equation (3)). Valence band (VB) holds h^+ and conduction band (CB) carries e^- .



The h^+ in VB plays a key role in generating hydroxyl radicals from H_2O molecules or hydroxyl ions (Equation (4)).



On the other hand, e^- in CB helps generate superoxide radicals from oxygen molecules (Equation (5)).

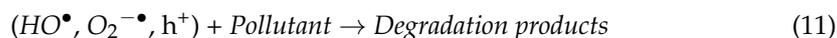


The produced superoxide radicals also help to generate hydroxyl radicals through a series of reactions (Equations (6)–(10)):



The resultant reactive oxygen species (ROS; $O_2^{\bullet-}$, HO^\bullet) is the key component in the photocatalytic deterioration of pollutants. The dye reacts with ROS and undergoes an oxidation reaction to form degradation products. The h^+ in VB can directly oxidize

the contaminant molecules and accelerate the photocatalytic activity of ZCG. Finally, the deterioration of organic pollutants by ZCG occurs as in Equation (11).



3. Materials and Methods

3.1. Materials

Copper(II) sulfate pentahydrate (99%) was received from Showa Chemical Co. Ltd., Japan (Akasaka, Minato-ku, Tokyo). Zinc acetate dihydrate (99.0%), urea (99.0–100.5%), sodium hydroxide (NaOH, 97%), ethyl alcohol (99.5%), and CR were purchased from Sigma-Aldrich (St. Louis, MO, USA). MB was received from Alfa Aesar (Heysham, Lancashire, UK).

3.2. Synthesis of CuO Nanoparticles

The CuO nanoparticles (CuO-NPs) were synthesized via the chemical precipitation method followed by high-pressure annealing. First, 2 g of $\text{CuSO}_4 \cdot 5\text{H}_2\text{O}$ was dissolved in 10 mL of distilled water. In the clear mixture, aqueous NaOH solution was mixed dropwise up to pH 11. The formation of precipitate was observed. The resultant mixture was stirred using a magnetic stirrer for 3 h at 600 rpm. The color of the precipitate was converted to black from bluish-green. The precipitate was taken out by filtration after washing with distilled water. The sample was desiccated at 70 °C in an oven overnight. The obtained sample was poured into a quartz crucible and stoppered with a lid. The crucible was then positioned in a vacuum chamber which was closed by an airtight gasket made of copper (O_2 -free). The sealed chamber was then kept in the furnace and heated at a rate of 7.5 °C min^{-1} at 400 °C for 3h. The calcined compound was ground to obtain the fine powder nanoparticles and reserved for the next use.

3.3. Synthesis of ZnO Nanoparticles and g- C_3N_4 Nanosheet

Both the ZnO nanoparticles (ZnO-NPs) and g- C_3N_4 nanosheet were prepared through a solvent-free modified thermal method. For ZnO-NPs, 5 g of $\text{Zn}(\text{CH}_3\text{COO})_2 \cdot 2\text{H}_2\text{O}$ was poured into a quartz crucible and covered with a lid. The crucible was then positioned in a stainless-steel chamber (SUS314; diameter = 35 mm; length = 60 mm), which was subsequently sealed with an oxygen-free copper gasket (OFHC). The chamber was put into a furnace (KSL-1100X-S-UL-LD, Richmond, CA, USA) and heated at 450 °C for 7 h with a heat-up rate of 5 °C min^{-1} . After thermolysis, the furnace was kept undisturbed to cool slowly to ambient temperature to induce the uniform and smooth formation of ZnO-NPs. Next, the same described procedure for ZnO-NPs was used to prepare a g- C_3N_4 nanosheet; the differences were (i) 2 g of urea was used to prepare g- C_3N_4 nanosheet and (ii) the urea was heated at 520 °C for 380 min with a heating rate of 4 °C min^{-1} .

3.4. Synthesis of ZnO/CuO/g- C_3N_4 Nanocomposite

The ZnO/CuO/g- C_3N_4 nanocomposite was prepared by an efficient co-crystallization process. Initially, as-synthesized CuO, ZnO, and g- C_3N_4 at a 2:2:1 weight ratio were transferred into a beaker containing 40 mL distilled water as a solvent. Then, the resultant mixture was homogenized using a bath sonication for 30 min. After that, the aqueous solution was stirred vigorously for 2 h at 600 rpm using a magnetic stirrer at ambient temperature (26 °C) to produce a nanocomposite in which the constituent components were well distributed. The resultant mixture was then left untouched for 1 day for co-crystallization and kept undisturbed for an additional 2 days to allow the precipitate to settle. The upper 50% of solution (20 mL) was removed, and the remaining mixture was subjected to evaporation at 60 °C in the oven to drive off the solvent molecules completely. The collected, dried powder of the prepared composite was then ground smoothly and stored in a sealed vial for further use. The nanocomposite is denoted as ZCG.

3.5. Instrumentation

An X-ray diffractometer (X'Pert PRO, PANalytical, Lelyweg, Almelo, The Netherlands) equipped with a Cu K α ($\lambda = 1.5406 \text{ \AA}$) radiation source was applied to inspect the crystal structure of the compounds. The chemical composition, oxidation state, and binding energies of the sample were analyzed by X-ray photoelectron spectroscopy (XPS, NEXSA, Thermo Fisher Scientific, East Grinstead, West Sussex, UK). The functional groups of the materials were examined by Fourier transform infrared (FTIR) spectroscopy (Thermo Fisher Scientific, Nicolet iS5). The morphological properties of the composite were evaluated by field-emission scanning electron microscopy (FE-SEM, SU8230, Hitachi, Minato-ku, Tokyo, Japan) and high-resolution transmission electron microscopy (HR-TEM, JEM-2200FS, JEOL, Akishima, Tokyo, Japan). To assess the optical features and bandgaps of the materials, a UV-vis spectrophotometer (Perkin Elmer Lambda 25, Ayer Rajah, Singapore) was used.

3.6. Measurements of Photocatalytic Performance

The photocatalytic proficiency of all the compounds was assessed by measuring the degradation of MB as a target contaminant. The assessments were driven using a xenon lamp (300 W) as a source of visible light. Additionally, a UV cut-off filter ($\geq 400 \text{ nm}$) was engaged to avoid UV irradiation. In a typical experiment, 0.020 g of sample was added into 100 mL of dye solution (20 mg L^{-1}). The resultant suspension was then ultrasonicated for 60 min to confirm the adsorption of dye molecules onto the catalyst surface. Further, this mixture was kept in dark conditions for 30 min to acquire an adsorption-desorption equilibrium. The photodegradation reaction was then started by contact with the assistance of a light source. Before and after the solar irradiation, the change in the dye concentration during the reaction was observed by UV-vis spectrophotometer. For measuring the absorbance of the samples, a constant volume of solution was measured at regular intervals. In addition, the photodegradation proficiency for CR was tested under identical conditions. The photocatalytic investigation of all the samples was executed under uniform experimental conditions. The recyclability of the ZCG nanocomposite was evaluated using a similar procedure in each set. This was achieved by collecting the precipitated sample (after centrifugation) and washing it several times with distilled water. The sample was then dried at $100 \text{ }^\circ\text{C}$ for approximately 5 h in a preheated furnace for successive evaluation of its recycling performance. Following this, the dry sample was used for the next cycle of the photocatalytic reaction.

4. Conclusions

ZnO/CuO/g-C₃N₄ nanocomposite was successfully synthesized through a cost-effective, facile co-crystallization method. The prepared nanocomposite was used to treat wastewater containing organic pollutants through visible light illumination and the product's durability and recycling capability was evaluated. The structural and morphological observation confirmed the nanocomposite was perfectly constructed. The top-most photocatalytic activity was observed for the ZCG nanocomposite, which induced 97.46% photodegradation of MB under visible light within 50 min. The ZCG nanocomposite showed 753%, 392%, 156%, and 130% higher photocatalytic efficiency compared with photolysis, g-C₃N₄, CuO-NPs, and ZnO-NPs, respectively. The photodeterioration of MB followed pseudo-first-order reaction kinetics and the k value of the ZCG composite was 23.6, 11.6, 3.4, and 2.4 times greater than those of photolysis, g-C₃N₄, CuO-NPs, and ZnO-NPs, respectively. The pH_{PZC} of our as-synthesized ZCG affirmed the anionic nature of the surface at a higher pH and correspondingly showed a cationic nature at lower pH. In addition, the photocatalytic activity and reaction kinetics of the ZCG composite for the deterioration of CR were investigated and the results were found to be remarkable. The outstanding photocatalytic performance was observed due to heterojunction formation among the g-C₃N₄, CuO-NPs, and ZnO-NPs compounds, which minimized the photogenerated e^- - h^+ pair recombination, and increased the electron flow rate. After six consecutive runs, the ZCG product showed excellent stability and recycling performance, confirmed by

employing XRD and FTIR analysis of the reused ZCG sample. Therefore, the overall results indicate that the ZCG nanocomposite could be practically used for visible-light-driven wastewater treatment; this sheds new light on the field of catalysts.

Supplementary Materials: The following supporting information can be downloaded at: <https://www.mdpi.com/article/10.3390/catal12020151/s1>, Figure S1: Linear plots of modified Scherrer equation (a) CuO-NPs, (b) ZnO-NPs, and (c) ZCG nanocomposite.

Author Contributions: Conceptualization, M.A.H. and J.A.; methodology, M.A.H.; software, M.A.H.; formal analysis, M.A.H., J.A. and Y.S.K.; investigation and data curation, M.A.H.; writing—original draft preparation, M.A.H.; writing—review and editing, M.A.H., J.A., Y.S.K., H.G.K., J.R.H. and L.K.K.; visualization, H.G.K., J.R.H. and L.K.K.; supervision, L.K.K.; project administration, L.K.K.; funding acquisition, L.K.K. All authors have read and agreed to the published version of the manuscript.

Funding: This research was supported by the Basic Science Research Program through the National Research Foundation of Korea (NRF) funded by the Ministry of Education (2016R1A6A1A03012069, 2018R1D1A1B07050752). This research was also supported by the Korean Government (NRF-2021R1I1A3045310).

Data Availability Statement: The data are available by corresponding author.

Conflicts of Interest: The authors declare no conflict of interest.

References

1. Akter, J.; Sapkota, K.P.; Hanif, M.A.; Islam, M.A.; Abbas, H.G.; Hahn, J.R. Kinetically controlled selective synthesis of Cu₂O and CuO nanoparticles toward enhanced degradation of methylene blue using ultraviolet and sun light. *Mater. Sci. Semicond. Process.* **2021**, *123*, 105570. [CrossRef]
2. Yang, Y.; Ali, N.; Khan, A.; Khan, S.; Khan, S.; Khan, H.; Xiaoqi, S.; Ahmad, W.; Uddin, S.; Ali, N.; et al. Chitosan-capped ternary metal selenide nanocatalysts for efficient degradation of Congo red dye in sunlight irradiation. *Int. J. Biol. Macromol.* **2021**, *167*, 169–181. [CrossRef] [PubMed]
3. Crini, G.; Lichtfouse, E. Advantages and disadvantages of techniques used for wastewater treatment. *Environ. Chem. Lett.* **2019**, *17*, 145–155. [CrossRef]
4. Akter, J.; Hanif, M.A.; Islam, M.A.; Sapkota, K.P.; Hahn, J.R. Selective growth of Ti³⁺/TiO₂/CNT and Ti³⁺/TiO₂/C nanocomposite for enhanced visible-light utilization to degrade organic pollutants by lowering TiO₂-bandgap. *Sci. Rep.* **2021**, *11*, 9490. [CrossRef] [PubMed]
5. He, X.; Yang, D.P.; Zhang, X.; Liu, M.; Kang, Z.; Lin, C.; Jia, N.; Luque, R. Waste eggshell membrane-templated CuO-ZnO nanocomposites with enhanced adsorption, catalysis and antibacterial properties for water purification. *Chem. Eng. J.* **2019**, *369*, 621–633. [CrossRef]
6. Bharathi, P.; Harish, S.; Archana, J.; Navaneethan, M.; Ponnusamy, S.; Muthamizhchelvan, C.; Shimomura, M.; Hayakawa, Y. Enhanced charge transfer and separation of hierarchical CuO/ZnO composites: The synergistic effect of photocatalysis for the mineralization of organic pollutant in water. *Appl. Surf. Sci.* **2019**, *484*, 884–891. [CrossRef]
7. Liu, Z.; Bai, H.; Xu, S.; Sun, D.D. Hierarchical CuO/ZnO “corn-like” architecture for photocatalytic hydrogen generation. *Int. J. Hydrog. Energy* **2011**, *36*, 13473–13480. [CrossRef]
8. Liu, C.; Meng, F.; Zhang, L.; Zhang, D.; Wei, S.; Qi, K.; Fan, J.; Zhang, H.; Cui, X. CuO/ZnO heterojunction nanoarrays for enhanced photoelectrochemical water oxidation. *Appl. Surf. Sci.* **2019**, *469*, 276–282. [CrossRef]
9. Saravanan, R.; Karthikeyan, S.; Gupta, V.K.; Sekaran, G.; Narayanan, V.; Stephen, A.J.M.S. Enhanced photocatalytic activity of ZnO/CuO nanocomposite for the degradation of textile dye on visible light illumination. *Mater. Sci. Eng. C* **2013**, *33*, 91–98. [CrossRef]
10. Khiavi, N.D.; Katal, R.; Eshkalak, S.K.; Masudy-Panah, S.; Ramakrishna, S.; Hu, J.Y. Visible light driven heterojunction photocatalyst of CuO-Cu₂O thin films for photocatalytic degradation of organic pollutants. *Nanomaterials* **2019**, *9*, 1011. [CrossRef]
11. Araújo, E.S.; da Costa, B.P.; Oliveira, R.A.P.; Libardi, J.; Faia, P.M.; de Oliveira, H.P. TiO₂/ZnO hierarchical heteronanostructures: Synthesis, characterization and application as photocatalysts. *J. Environ. Chem. Eng.* **2016**, *4*, 2820–2829. [CrossRef]
12. Pal, S.; Maiti, S.; Maiti, U.N.; Chattopadhyay, K.K. Low temperature solution processed ZnO/CuO heterojunction photocatalyst for visible light induced photo-degradation of organic pollutants. *Cryst. Eng. Comm.* **2015**, *17*, 1464–1476. [CrossRef]
13. Hossain, S.S.; Tarek, M.; Munusamy, T.D.; Karim, K.M.R.; Roopan, S.M.; Sarkar, S.M.; Cheng, C.K.; Khan, M.M.R. Facile synthesis of CuO/CdS heterostructure photocatalyst for the effective degradation of dye under visible light. *Environ. Res.* **2020**, *188*, 109803. [CrossRef] [PubMed]
14. Hassanpour, M.; Safardoust-Hojaghan, H.; Salavati-Niasari, M.; Yeganeh-Faal, A. Nano-sized CuO/ZnO hollow spheres: Synthesis, characterization and photocatalytic performance. *J. Mater. Sci. Mater. Electron.* **2017**, *28*, 14678–14684. [CrossRef]

15. Xu, L.; Zhou, Y.; Wu, Z.; Zheng, G.; He, J.; Zhou, Y. Improved photocatalytic activity of nanocrystalline ZnO by coupling with CuO. *J. Phys. Chem. Solids* **2017**, *106*, 29–36. [[CrossRef](#)]
16. Cahino, A.M.; Loureiro, R.G.; Dantas, J.; Madeira, V.S.; Fernandes, P.C.R. Characterization and evaluation of ZnO/CuO catalyst in the degradation of methylene blue using solar radiation. *Ceram. Int.* **2019**, *45*, 13628–13636. [[CrossRef](#)]
17. Zhu, W.; Sun, F.; Goei, R.; Zhou, Y. Construction of WO₃-g-C₃N₄ composites as efficient photocatalysts for pharmaceutical degradation under visible light. *Catal. Sci. Technol.* **2017**, *7*, 2591. [[CrossRef](#)]
18. Borthakur, S.; Basyach, P.; Kalita, L.; Sonowal, K.; Tiwari, A.; Chetia, P.; Saikia, L. Sunlight assisted degradation of a pollutant dye in water by a WO₃@g-C₃N₄ nanocomposite catalyst. *New J. Chem.* **2020**, *44*, 2947–2960. [[CrossRef](#)]
19. Peng, W.; Min, Y.; Sengpei, T.; Feitai, C.; Youji, L. Preparation of cellular C₃N₄/CoSe₂/GA composite photocatalyst and its CO₂ reduction activity. *Chem. J. Chin. Univ. -Chin.* **2021**, *42*, 1924–1932.
20. Lin, X.; Du, S.; Li, C.; Li, G.; Li, Y.; Chen, F.; Fang, P. Consciously constructing the robust NiS/g-C₃N₄ hybrids for enhanced photocatalytic hydrogen evolution. *Catal. Lett.* **2020**, *150*, 1898–1908. [[CrossRef](#)]
21. Tang, S.; Fu, Z.; Li, Y.; Li, Y. Study on boron and fluorine-doped C₃N₄ as a solid activator for cyclohexane oxidation with H₂O₂ catalyzed by 8-quinolinolato iron^{III} complexes under visible light irradiation. *Appl. Catal. A Gen.* **2020**, *590*, 117342. [[CrossRef](#)]
22. Chen, P.; Liu, F.; Ding, H.; Chen, S.; Chen, L.; Li, Y.J.; Au, C.T.; Yin, S.F. Porous double-shell CdS@C₃N₄ octahedron derived by *in situ* supramolecular self-assembly for enhanced photocatalytic activity. *Appl. Catal. B Environ.* **2019**, *252*, 33–40. [[CrossRef](#)]
23. Xiong, S.; Yin, Z.; Zhou, Y.; Peng, X.; Yan, W.; Liu, Z.; Zhang, X. The dual-frequency (20/40 kHz) ultrasound assisted photocatalysis with the active carbon fiber-loaded Fe³⁺-TiO₂ as photocatalyst for degradation of organic dye. *Bull. Korean Chem. Soc.* **2013**, *34*, 3039–3045. [[CrossRef](#)]
24. Singh, J.; Arora, A.; Basu, S. Synthesis of coral like WO₃/g-C₃N₄ nanocomposites for the removal of hazardous dyes under visible light. *J. Alloys Compd.* **2019**, *808*, 151734. [[CrossRef](#)]
25. Hanif, M.A.; Akter, J.; Lee, I.; Islam, M.A.; Sapkota, K.P.; Abbas, H.G.; Hahn, J.R. Formation of chemical heterojunctions between ZnO nanoparticles and single walled carbon nanotubes for synergistic enhancement of photocatalytic activity. *J. Photochem. Photobiol. A Chem.* **2021**, *413*, 113260. [[CrossRef](#)]
26. Zhang, Q.; Zhang, K.; Xu, D.; Yang, G.; Huang, H.; Nie, F.; Liu, C.; Yang, S. CuO nanostructures: Synthesis, characterization, growth mechanisms, fundamental properties. *Prog. Mater. Sci.* **2014**, *60*, 208–337. [[CrossRef](#)]
27. Shi, Y.; Yang, Z.; Liu, Y.; Yu, J.; Wang, F.; Tong, J.; Su, B.; Wang, Q. Fabricating a g-C₃N₄/CuO_x heterostructure with tunable valence transition for enhanced photocatalytic activity. *RSC Adv.* **2016**, *6*, 39774. [[CrossRef](#)]
28. Meng, J.; Pei, J.; He, Z.; Wu, S.; Lin, Q.; Wei, X.; Li, J.; Zhang, Z. Facile synthesis of g-C₃N₄ nanosheets loaded with WO₃ nanoparticles with enhanced photocatalytic performance under visible light irradiation. *RSC Adv.* **2017**, *7*, 24097–24104. [[CrossRef](#)]
29. Hanif, M.A.; Akter, J.; Islam, M.A.; Sapkota, K.P.; Hahn, J.R. Visible-light-driven enhanced photocatalytic performance using cadmium-doping of tungsten (VI) oxide and nanocomposite formation with graphitic carbon nitride disks. *Appl. Surf. Sci.* **2021**, *565*, 150541. [[CrossRef](#)]
30. Xiao, T.; Tang, Z.; Yang, Y.; Tang, L.; Zhou, Y.; Zou, Z. In situ construction of hierarchical WO₃/g-C₃N₄ composite hollow microspheres as a Z-scheme photocatalyst for the degradation of antibiotics. *Appl. Catal. B Environ.* **2018**, *220*, 417–428. [[CrossRef](#)]
31. Alman, V.; Singh, K.; Bhat, T.; Sheikh, A.; Gokhale, S. Sunlight assisted improved photocatalytic degradation of rhodamine B using Pd-loaded g-C₃N₄/WO₃ nanocomposite. *Appl. Phys. A* **2020**, *126*, 724. [[CrossRef](#)]
32. Zhao, D.; Wang, Y.; Dong, C.L.; Huang, Y.C.; Chen, J.; Xue, F.; Shen, S.; Guo, L. Boron-doped nitrogen-deficient carbon nitride-based Z-scheme heterostructures for photocatalytic overall water splitting. *Nat. Energy* **2021**, *6*, 388–397. [[CrossRef](#)]
33. Chen, C.; Zheng, Y.; Zhan, Y.; Lin, X.; Zheng, Q.; Wei, K. Reduction of nanostructured CuO bundles: Correlation between microstructure and reduction properties. *Cryst. Growth Des.* **2008**, *8*, 3549–3554. [[CrossRef](#)]
34. Akter, J.; Hanif, M.A.; Islam, M.A.; Sapkota, K.P.; Lee, I.; Hahn, J.R. Visible-light-active novel α-Fe₂O₃/Ta₃N₅ photocatalyst designed by band-edge tuning and interfacial charge transfer for effective treatment of hazardous pollutants. *J. Environ. Chem. Eng.* **2021**, *9*, 106831. [[CrossRef](#)]
35. Hanif, M.A.; Lee, I.; Akter, J.; Islam, M.A.; Zahid, A.A.S.M.; Sapkota, K.P.; Hahn, J.R. Enhanced photocatalytic and antibacterial performance of ZnO nanoparticles prepared by an efficient thermolysis method. *Catalysts* **2019**, *9*, 608. [[CrossRef](#)]
36. Dong, Z.; Wu, Y.; Thirugnanam, N.; Li, G. Double Z-scheme ZnO/ZnS/g-C₃N₄ ternary structure for efficient photocatalytic H₂ production. *Appl. Surf. Sci.* **2018**, *430*, 293–300. [[CrossRef](#)]
37. Jourshabani, M.; Shariatnia, Z.; Badiei, A. High efficiency visible-light-driven Fe₂O₃-xS_x/S-doped g-C₃N₄ heterojunction photocatalysts: Direct Z-scheme mechanism. *J. Mater. Sci. Technol.* **2018**, *34*, 1511–1525. [[CrossRef](#)]
38. Thomas, M.; Naikoo, G.A.; Sheikh, M.U.D.; Bano, M.; Khan, F. Effective photocatalytic degradation of Congo red dye using alginate/ carboxymethyl cellulose/TiO₂ nanocomposite hydrogel under direct sunlight irradiation. *J. Photochem. Photobiol. A Chem.* **2016**, *327*, 33–43. [[CrossRef](#)]